PERGAMON

Journal of Structural Geology 24 (2002) 1413–1429

JOURNAL OF STRUCTURAL GEOLOGY

www.elsevier.com/locate/jstrugeo

Normal fault growth in layered rocks at Split Mountain, Utah: influence of mechanical stratigraphy on dip linkage, fault restriction and fault scaling

Scott J. Wilkins*, Michael R. Gross

Department of Geology, Florida International University, Miami, FL 33199, USA

Received 25 February 2000; revised 18 June 2001; accepted 28 September 2001

Abstract

We analyze displacement profiles measured from a population of normal faults that cut across layered clastic rocks, in order to investigate the controls of mechanical layering on fault growth. Abundant fault tips and displacement minima are found at lithologic contacts, and in some cases are associated with relay structures, suggesting that lithology is responsible for controlling the location of vertical, along-dip segment linkage. Based on the locations and distributions of displacement minima and maxima within the stratigraphic section, as well as the distribution of small faults, we conclude that: (1) most faults initiate within shale beds, and (2) lithologic contacts restrict fault growth at a variety of scales. One consequence of fault restriction is the development of high displacement gradients at fault tips. Because fault tips are only temporarily pinned at bed boundaries, the degree of restriction will fluctuate as faults propagate through the section. In general, maximum displacement (D_{max}) across the faults correlates with cross-sectional trace length (L). The D_{max}/L ratio decreases as a function of percent shale offset by a fault, and increases as a function of near-tip displacement gradient. An empirically-derived equation relates D_{max}/L to rock composition and fault tip displacement gradients, thereby providing a mechanism to predict fault dimensions in the subsurface from limited data.

Keywords: Normal fault growth; Fault scaling; Dip-linkage; Displacement gradients; Mechanical stratigraphy

1. Introduction

Displacement distributions provide insight into the propagation and slip history along faults, and therefore, to the fundamental physics that govern fault growth (e.g. Walsh and Watterson, 1987, 1988; Cowie and Scholz, 1992a; Bürgmann et al., 1994). Determining the key factors that influence displacement distributions is thus essential to developing a comprehensive model for fault growth (e.g. Bürgmann et al., 1994; see review in Schultz, 2000). In this paper we analyze displacements along normal faults within mechanically layered rocks in order to assess the role of lithology in controlling fault development.

The most detailed displacement profiles to date have been derived from normal fault scarps by measuring the net displacement or throw of a single marker horizon along fault strike (e.g. Opheim and Gudmundsson, 1989; Dawers et al., 1993; Schlische et al., 1996; Cartwright and Mansfield, 1998; Cowie and Shipton, 1998; Moore and Schultz, 1999). For cases of complete exposure, this methodology provides a nearly continuous stream of data points, thus resulting in accurate profiles, especially in critical areas such as near fault tips. Consequently, such profiles have proven essential for understanding processes associated with along-strike segment linkage (Peacock, 1991; Peacock and Sanderson, 1991; Dawers and Anders, 1995; Willemse et al., 1996) as well as for fault growth models based on displacement distributions near fault tips (Cowie and Scholz, 1992a; Cartwright and Mansfield, 1998; Cowie and Shipton, 1998). However, along-strike displacement profiles of normal faults do not commonly reveal significant effects of mechanical layering on fault growth. Such effects may result from differences in mechanical properties among the layers (Muraoka and Kamata, 1983; Peacock, 1991; Bürgmann et al., 1994; Childs et al., 1996), and include changes in fault dip as a function of lithology (Peacock and Zhang, 1994; Wilkins, 1999), restriction of fault growth imposed by lithologic barriers (Rippon, 1985;

* Corresponding author. Present address: Geomechanics–Rock Fracture Group, Department of Geology, University of Nevada, Mackay School of Mines 172, Reno, NV 89557-0138, USA. Tel.: +1-702-784-6050; fax: +1-702-784-1833.

E-mail address: swilki@unr.edu (S.J. Wilkins).

0191-8141/02/$ - see front matter
PII: S0191-8141(01)00154-7

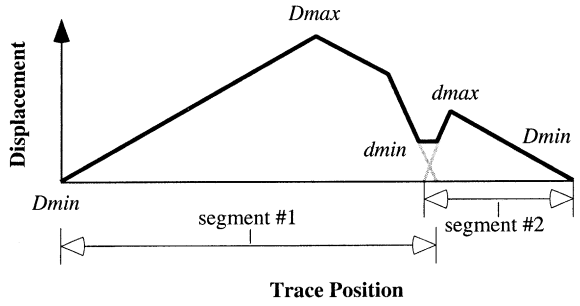

Fig. 1. Schematic displacement profile illustrating the terminology used for various attributes (i.e. D_{max}, d_{max}, D_{min}, and d_{min}) as well as the identification of individual fault segments. A local displacement minimum (d_{min}) is often found where two initially isolated segments have subsequently linked together.

Gross, 1995; Childs et al., 1996; Nicol et al., 1996), and the presence of detachments and other structures that may influence fault growth and linkage (Wojtal, 1994, 1996; Gross et al., 1997a,b). These effects are primarily recognized in cross-sectional displacement profiles of normal faults, although such profiles are inherently limited because they rely upon a discrete number of displaced markers as the source of data, rather than a continuously exposed fault scarp. Although displacement profiles in cross-section

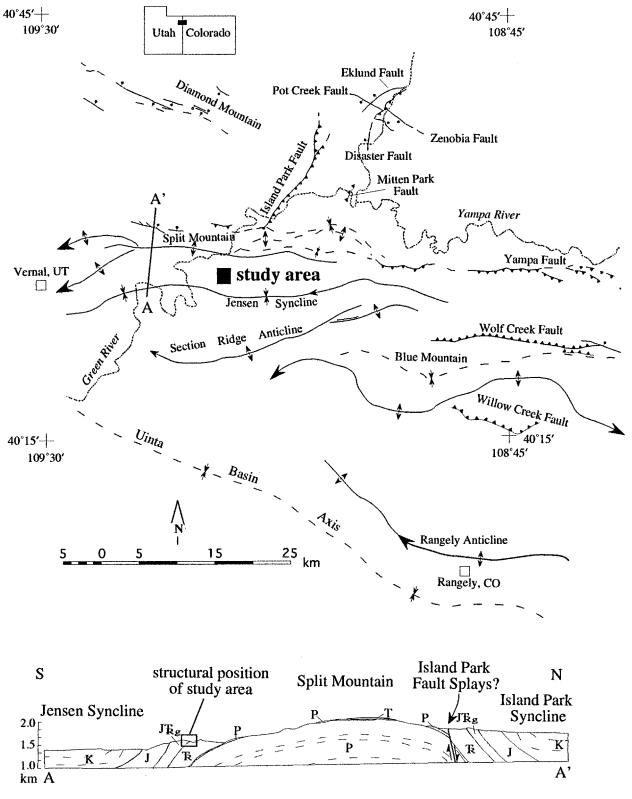

Fig. 2. Structure map and cross-section of the southeast Uinta Mountains, NE Utah. The outcrop is located on the southern flank of Split Mountain Anticline (UTM 12, 4476140N, 653880W). Modified from Rowley et al. (1985) and Untermann and Untermann (1965).

have been constructed for normal faults in layered rocks (Muraoka and Kamata, 1983; Childs et al., 1996; Mansfield and Cartwright, 1996; Gross et al., 1997c), displacement distribution characteristics (i.e. displacement minima, maxima, gradients) have not been systematically correlated to specific lithologic units and their boundaries in outcrop (i.e. mechanical stratigraphy).

Isolated faults often link together to form larger faults through the process of segment linkage. Segment linkage has been established as an important mechanism for fault growth at the centimeter–kilometer scale through the analysis of incremental slip (i.e. coseismic, e.g. Yielding et al., 1981; Caskey et al., 1996) and cumulative displacement distributions (Ellis and Dunlap, 1988; Peacock, 1991; Peacock and Sanderson, 1991; Dawers and Anders, 1995; Cartwright et al., 1995; Mansfield and Cartwright, 1996; Willemse et al., 1996; Gross et al., 1997c; Morley, 1999). By definition, displacement is zero at the fault tips and increases to a maximum somewhere between the fault tips (Fig. 1; Elliot, 1976; Muraoka and Kamata, 1983; Rippon, 1985; Walsh and Watterson, 1987; Dawers et al., 1993). Therefore, a fault comprised of two initially isolated segments that have subsequently linked together is often marked by a local displacement minimum between two maxima; the minimum displacement may represent the location of fault linkage (Fig. 1; Yielding et al., 1981; Ellis and Dunlap, 1988; Peacock, 1991; Peacock and Sanderson, 1991; Cartwright et al., 1995; Dawers and Anders, 1995; Caskey et al., 1996). To date, only a few studies have attempted to evaluate the factors that control the vertical segmentation of normal faults (Childs et al., 1996; Mansfield and Cartwright, 1996), or discuss the implications of vertical segmentation in terms of fault scaling properties (Ackermann et al., 2001).

The main goal of this paper is to better understand the development of normal fault systems in mechanically layered rocks. Specifically, by correlating characteristics of fault displacement distributions and geometry with a detailed mechanical stratigraphy, we attempt to identify stratigraphic intervals where faults initiate, terminate, and link together. We then investigate the importance of host rock rheology and the restriction of fault propagation by mechanical layer boundaries in controlling displacement–length scaling relationships.

2. Geologic setting

We conducted a structural analysis along the southern flank of Split Mountain Anticline (SMA), an ~E–W-trending Laramide structure in the southeast portion of the Uinta Mountains in northeast Utah (Fig. 2). The outcrop is located approximately 1 km west of Josie's Ranch historical site within Dinosaur National Monument. Rowley and Hansen (1979) attribute the formation of SMA to reverse slip on the Island Park fault (Fig. 2), some of whose

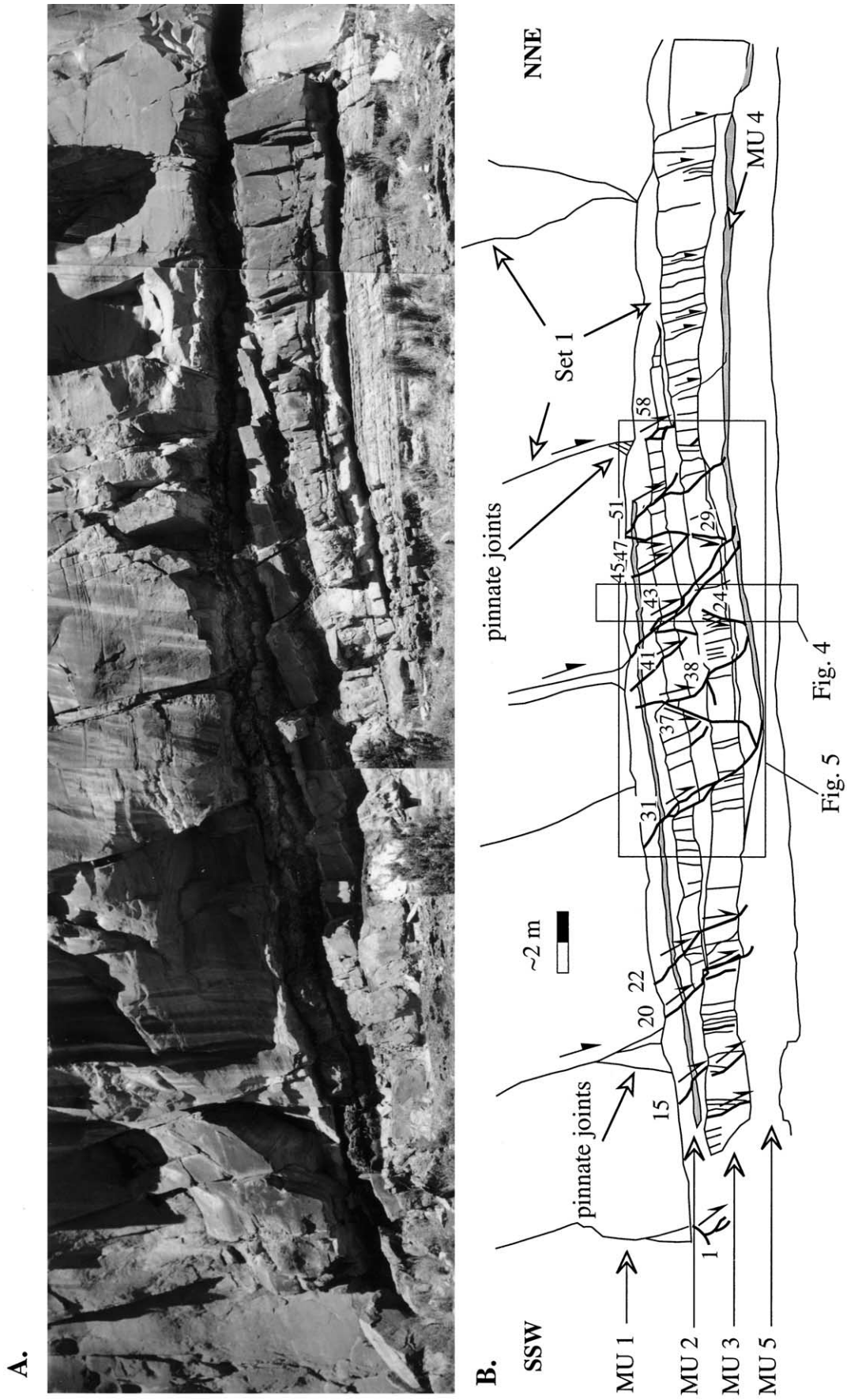

Fig. 3. (A) Photo-mosaic of faulted area of the outcrop. (B) Cross-sectional sketch of joints (thin lines) and faults (thick lines) mapped from the outcrop (solid arrows indicate shear sense). Major, throughgoing faults are identified by number; MU refers to major mechanical units in the section (see Fig. 4).

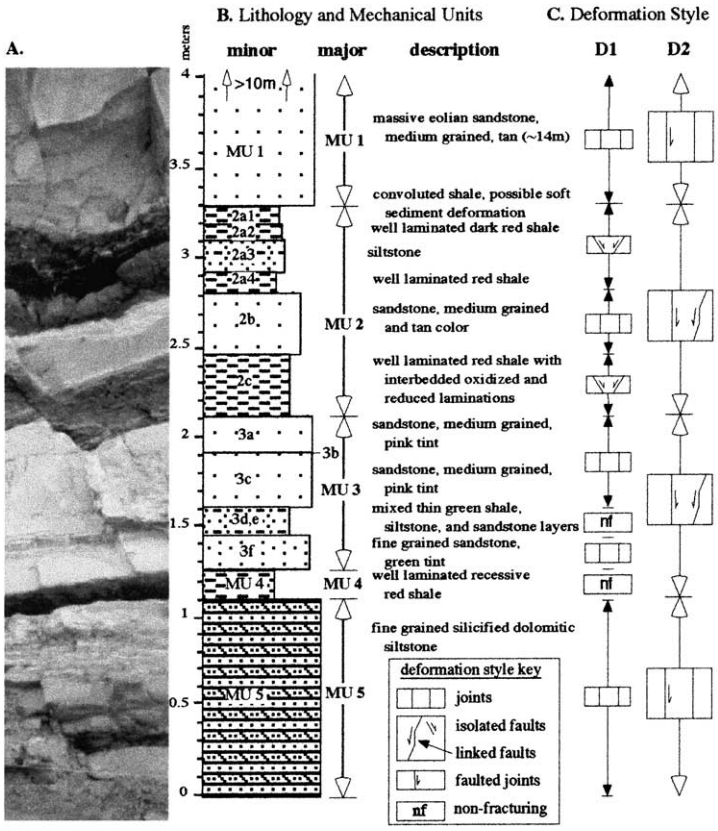

Fig. 4. Typical section of mechanical stratigraphy at the Josie's Ranch outcrop consisting of (A) photograph, (B) lithologic description, and (C) deformation style for D1 and D2. Structures are confined to minor mechanical units during D1 but span major mechanical units during D2.

associated smaller splay faults outcrop on the northern flank of SMA. A kinematic analysis of mesoscale faults in the cover rocks surrounding SMA by Gregson and Erslev (1997) suggests a regional NNW–SSE trending maximum principal stress during folding. Folding of the sedimentary cover and subsequent erosion exposed a succession of Mesozoic and upper Paleozoic rocks on both limbs (Rowley and Hansen, 1979). Forced-folding over basement faults, a common mechanism for fold development in Laramide-style structures, may cause the sedimentary cover in the upper portion of the fold to extend, while contraction occurs along the underlying basement faults (McConnell and Wilson, 1993; Engelder et al., 1997). Manifestations of extension within the tilted cover rocks at Split Mountain include the formation and selective reactivation of brittle structures such as joints and normal faults (Wilkins et al., 2001; Silliphant et al., 2002).

3. Outcrop description

The outcrop consists of a massive 10–15-m-thick eolian sandstone bed that overlies ~0.1–1-m-thick interbedded sandstone, siltstone and shale beds. The cliff-forming massive sandstone bed belongs to the Glen Canyon Sandstone of upper Triassic–lower Jurassic age, whereas the thinner interbeds of sandstone, siltstone and shale belong to the lower Triassic Chinle Formation (Fig. 3A; Rowley and Hansen, 1979). Weathering of the outcrop has resulted in a vertical cliff that trends NNE–SSW (i.e. orthogonal to the fold axis of Split Mountain) and dips roughly 18° to the SSW. Normal faults measured in this study are preferentially localized within a distinct lens of shale-dominated beds beneath the thick, uppermost sandstone bed (Fig. 3).

3.1. Mechanical stratigraphy

Mechanical units within the outcrop were identified and described according to their lithology, thickness and style of brittle deformation. The resulting section (Fig. 4) defines a 'mechanical stratigraphy', which relates deformation style and intensity to individual mechanical units (Corbett et al., 1987; Gross, 1995; Gross et al., 1997a,b; Fischer and Jackson, 1999). A mechanical unit does not necessarily correspond to a lithologic unit because: (1) several lithologic units may deform as a single mechanical unit, (2) a single lithologic unit may be comprised of several mechanical units, (3) mechanical units may be defined by structural contacts rather than lithologic contacts, and (4) mechanical units may be defined at different scales within the same outcrop, as is the case in this study.

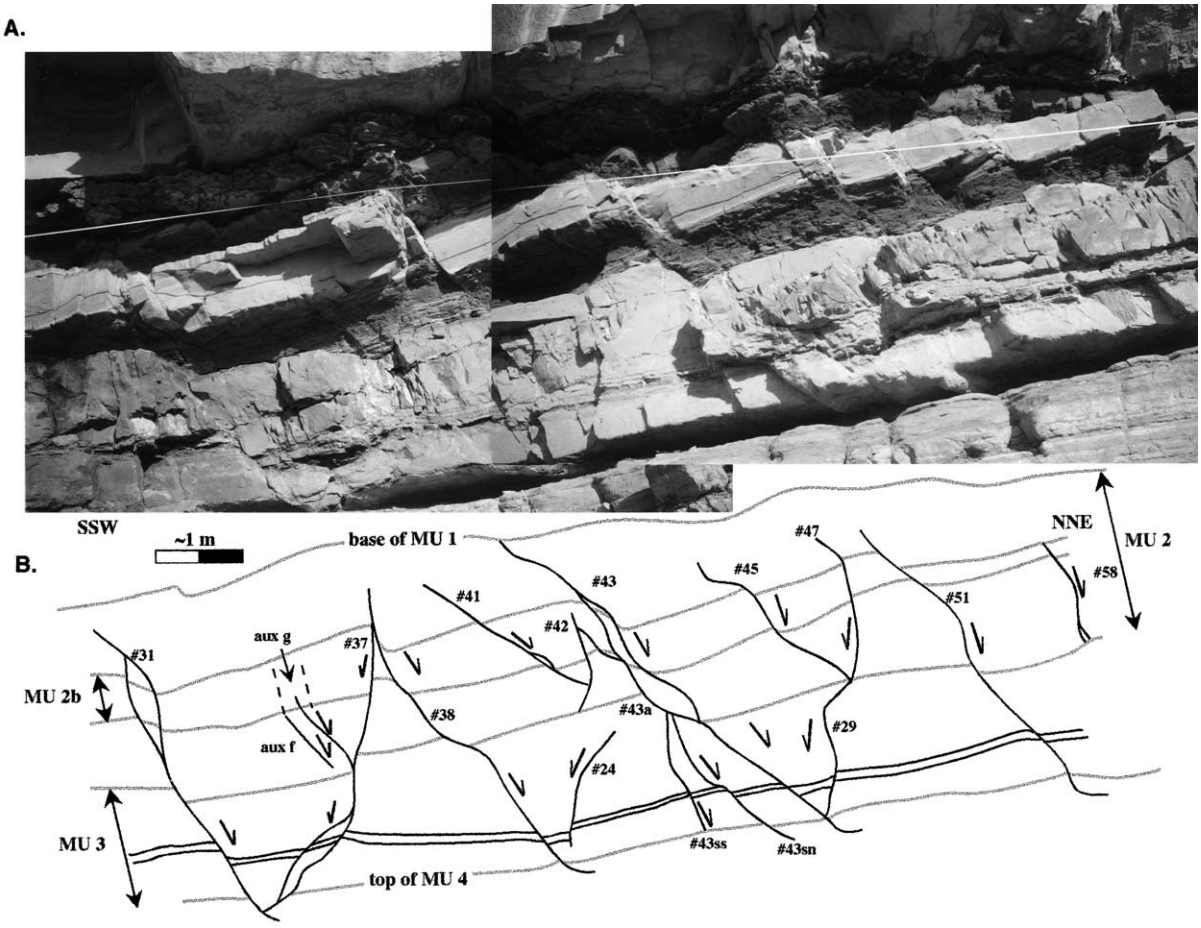

Fig. 5. (A) Outcrop photograph and (B) sketch of faults (solid black lines, arrows indicate shear sense) in the most intensely faulted region of the outcrop. Joints (dotted black lines) are mostly omitted for clarity. Thick gray lines are stratigraphic markers bounding MU 2b and MU 3. Individual faults are identified by number.

The outcrop is divided into five major mechanical units, of which two (MU 2 and MU 3) are further subdivided into minor mechanical units. The main lithologies, listed in order of decreasing competency, are silicified dolomitic siltstone, sandstone, siltstone, and shale. Deformation styles include joints, faults, faulted joints (i.e. faults that originated as joints) and non-fractured units. The first phase of deformation (D1) occurred while bedding was horizontal and resulted in the formation of faults and joints confined to separate and individual mechanical units (Fig. 4; Wilkins et al., 2001). Of these early structures, faults are preferentially located in the shale and siltstone beds, whereas joints occur within the sandstone and silicified dolomitic siltstone beds. The second phase of deformation (D2) is associated with the southward tilting of strata during the formation of Split Mountain anticline (Fig. 2), and resulted in the formation of throughgoing faults and the faulting of pre-existing joints (Fig. 4; Wilkins et al., 2001). Throughgoing faults cross multiple minor mechanical units and are either confined to MU 2 (see faults 15, 41, 45, 47 and 58 in Fig. 3) or MU 3 (see faults 24 and 29 in Fig. 3), span from MU 2 to MU 4 (see faults 22, 31, 37, 38, and 51 in Fig. 3), or in some instances have linked together with large joints initially confined to MU 1 (see faults 20 and 43 in Fig. 3). Many of the throughgoing faults terminate down-dip into MU 4, a recessive shale bed that serves as a structural detachment between two thicker and more competent mechanical units (Figs. 3 and 4). The wide range of cross-sectional fault lengths at this outcrop provides an opportunity to consider differences in displacement distributions at various stages of fault growth.

We measured the distance between upper and lower tips of the normal faults in cross-section. We refer to this down-dip dimension of the normal fault as the ‘cross-sectional trace length’. Among the faults measured, cross-sectional lengths range from ~20 to 500 cm. Displacements across the faults range from 0.5 to 40 cm. Fault dips are rarely uniform along large faults or fault zones, often refracting to steeper or shallower angles at the contacts of adjoining mechanical units (e.g. faults 37 and 38, Fig. 5). In order to more accurately characterize the range in fault geometry, orientation measurements were taken at various positions

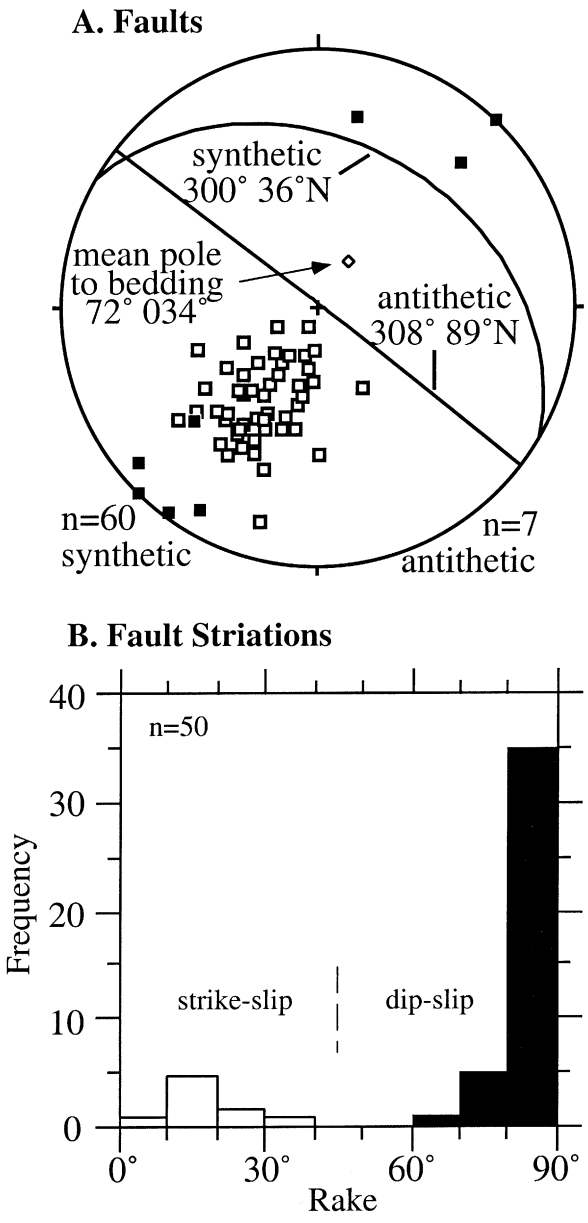

Fig. 6. (A) Lower hemisphere, equal-area projection of poles to synthetic (hollow squares) and antithetic (solid squares) faults. Multiple poles are plotted for faults whose orientation changes within the section. (B) Histogram of rake angles measured from fault striations.

along the lengths of refracted faults. The orientation of each fault segment appears in the stereoplot of Fig. 6A. The faults form a conjugate geometry that define a series of horst and graben structures. The large multi-layer fault zones group into a dominant north-dipping set (thus referred to as synthetic) and a less abundant and subvertical antithetic set (Fig. 6A). All faults exhibit normal stratigraphic separations and where observable, dip-slip motion indicators predominate on both faults and faulted joints (Fig. 6B), indicating that measured displacements reflect true displacements (Wojtal, 1996).

4. Analysis of fault displacement distributions and fault dimensions

4.1. Measuring techniques, profile construction and nomenclature

Displacements, trace lengths, and positions of offset marker horizons were measured in cross-section along the traces of 40 normal faults. Displacement distribution profiles were constructed for 14 throughgoing faults that display clear geometries in outcrop and have a sufficient number of offset marker horizons to generate accurate displacement profiles. The measurement error is estimated as 1.5 cm. Displacement profiles were first determined for individual fault segments or splays and then combined together into a cumulative profile for each fault zone. The profiles are correlated to the mechanical stratigraphy with boundaries and lithologies indicated for each unit (Fig. 7). Positions of marker horizons are plotted at the midpoint between offset blocks and the left-hand side of all profiles represents the stratigraphic position of the upper fault tip. We define D_{max} as the greatest amount of displacement measured along the fault zone, whereas d_{max} is a local maximum represented by an isolated peak that is less than D_{max} (Fig. 1). We thus define d_{min} as a local minimum that occurs between two maxima. The absolute minimum (D_{min}) occurs only at the fault tips where displacement is zero (Fig. 1).

Displacement distributions along two fault systems are described in an effort to illustrate the structural significance of displacement minima and differences in the degree of development among the faults. The displacement profile for faults 29 and 47 (Figs. 5 and 7) consists of two separate peaks. Each peak represents a distinct fault segment; one occurs within MU 3 and another within MU 2. Although the faults are physically connected at the MU 2–MU 3 boundary, displacements decrease to zero at the intersection. This fault geometry and displacement pattern is interpreted to represent an initial stage of segment linkage. In contrast, fault 31 (Fig. 5) is at a more advanced stage of development. Three distinct maxima are apparent (Fig. 7), where the central displacement peak is separated by d_{mins} that exhibit approximately 80% of the displacement at the maxima. Fault 31 consists of two fault traces within the region that spans from the upper to lower d_{min}, thus defining a fault lens (Fig. 5) that may represent a breached relay ramp between two previously isolated segments (Childs et al., 1995). Both geometry and displacement patterns therefore indicate that initially isolated segments have linked to form a throughgoing fault.

4.2. Controls on fault terminations and near-tip displacement gradients

By analyzing the spatial relationships among fault tips and adjacent structures, we seek to identify the predominant type of discontinuity responsible for inhibiting fault

propagation. Fig. 8 displays the frequency of fault tips that abut: (1) bed contacts, (2) adjacent faults, (3) both bed contacts and faults at the same location, or (4) occur within beds, and thus are not in physical contact with any observable mechanical boundaries. The distribution is highly skewed, with the largest frequency of fault tips occurring at bed contacts. Of the 10 fault tips that occur between bed boundaries (i.e. within beds in Fig. 8), seven are located within the detachment horizon (MU 4). The lowest frequency ($n = 3$) of fault tips terminate against neighboring faults alone, whereas eight additional fault tips terminate against both neighboring faults and bed contacts at the same location. The abundance of fault tips located at bed contacts suggests that stratigraphic layering acts to inhibit or restrict fault propagation. For a fault to propagate beyond the mechanical barrier, additional slip must first accumulate, thereby creating high displacement gradients adjacent to fault tips (Nicol et al., 1996; Gupta and Scholz, 2000). We test this hypothesis by analyzing differences in near-tip displacement gradients as a function of the tip environments classified above.

Displacement gradients (i.e. the change in displacement as a function of distance along the fault) are calculated from the fault tips to the first measured point, similar to the method of Cartwright and Mansfield (1998). On average, the distance between the first measured point and the tip is less than 20% of the fault half-length, i.e. within the region (approximately $<$10–20%) where tip gradients are presumably most sensitive to local heterogeneities (Cowie and Shipton, 1998). In some cases, displacement gradients along the profiled fault tips exhibit clear differences that are dependent upon the tip environment (Fig. 8A). For instance, displacement gradients along fault tips that have listric geometries within MU 4 are lower, on average, than gradients along fault tips that abut against observable discontinuities (Fig. 9A). In contrast, the type of discontinuity (e.g. bed contacts, faults or faults at bed contacts) does not seem important because the displacement gradient magnitudes are not a clear function of the different mechanical boundaries. Interestingly, relatively low gradients (i.e. $< \sim 0.2$) also exist along fault tips that abut against mechanical boundaries. Although these tips may seem restricted from propagating beyond the boundary, no physical consequence of restricted propagation is observable in the form of abnormally large (i.e. $> \sim 0.4$) displacement gradients (Rippon, 1985; Peacock, 1991; Peacock and Sanderson, 1991; Nicol et al., 1996; Willemse et al., 1996; Gupta and Scholz, 2000). Consequently, we suggest that restricted faults should be defined not only by the occurrence of a fault tip in physical contact with a mechanical boundary, but also by abnormally large near-tip displacement gradients.

Bed-contact restrictors are further analyzed in order to decipher lithologic controls on fault propagation. For example, we expect that faults propagating through a shale bed may be restricted from propagating into an adjacent sandstone bed. In contrast, a fault propagating through a sandstone bed might propagate unhindered into a shale bed. We classify three types of bed-contact boundaries where fault tips are located (Fig. 8A): a fault that propagates from a sandstone to a shale (a), from a shale to a sandstone (b), and from a shale to a shale (c). Three observations can be drawn from these data (Fig. 9B). First, near-tip displacement gradients are relatively low when tips are located at shale–shale contacts. Second, very few tips (only one was observed) are restricted from propagating from sandstone beds into shale beds. Finally, tips that propagate through a shale bed and terminate at a sandstone contact exhibit a wide range of displacement gradients, but include the largest near-tip gradients.

In summary, it is apparent that the more competent sandstone beds, or the contacts surrounding sandstone beds, are the predominant restrictors to fault propagation at this outcrop. However, not all faults that terminate at sandstone contacts exhibit large near-tip displacement gradients, suggesting they have not *yet* become restricted from propagating.

4.3. Factors influencing scaling of displacement with cross-sectional trace length

Unfortunately the phrase ‘fault length’ has not been consistently defined in the structural geology literature (Peacock et al., 2000). Some workers define fault length as the dimension parallel to the slip vector (e.g. Watterson, 1986; Walsh and Watterson, 1988), so that the length of a normal fault would be equivalent to the dip dimension. Other workers have defined fault length as the trace length in map view, i.e. the strike dimension (e.g. Dawers et al., 1993; Cartwright et al., 1995; Poulimenos, 2000). At issue here is whether or not displacement–length scaling relations have been established for lengths measured in the dip direction as well as for lengths measured in the strike dimension. Theoretical considerations suggest that displacements are distributed in three dimensions along a fully bounded fault (Willemse et al., 1996; Schultz and Fossen, 2002), and consequently, D_{max} is expected to scale with length when measured in both the strike and dip dimensions. More importantly, fault data collected in cross-sectional exposures reveal that displacement may scale with cross-sectional trace length for dip-slip faults in layered rocks (Muraoka and Kamata, 1983; Doutsos and Poulimenos, 1992; Gross et al., 1997b; Wilkins et al., 2001). Furthermore, displacement–length data measured in cross-section are commonly included within global data compilations used to establish scaling relations over many orders of magnitude (e.g. Walsh and Watterson, 1988; Marrett and Allmendinger, 1991; Cowie and Scholz, 1992a,b; Clark and Cox, 1996; Peacock and Sanderson, 1996; Schlische et al., 1996). Thus, we conclude that the analysis of fault displacement and length scaling relations measured in

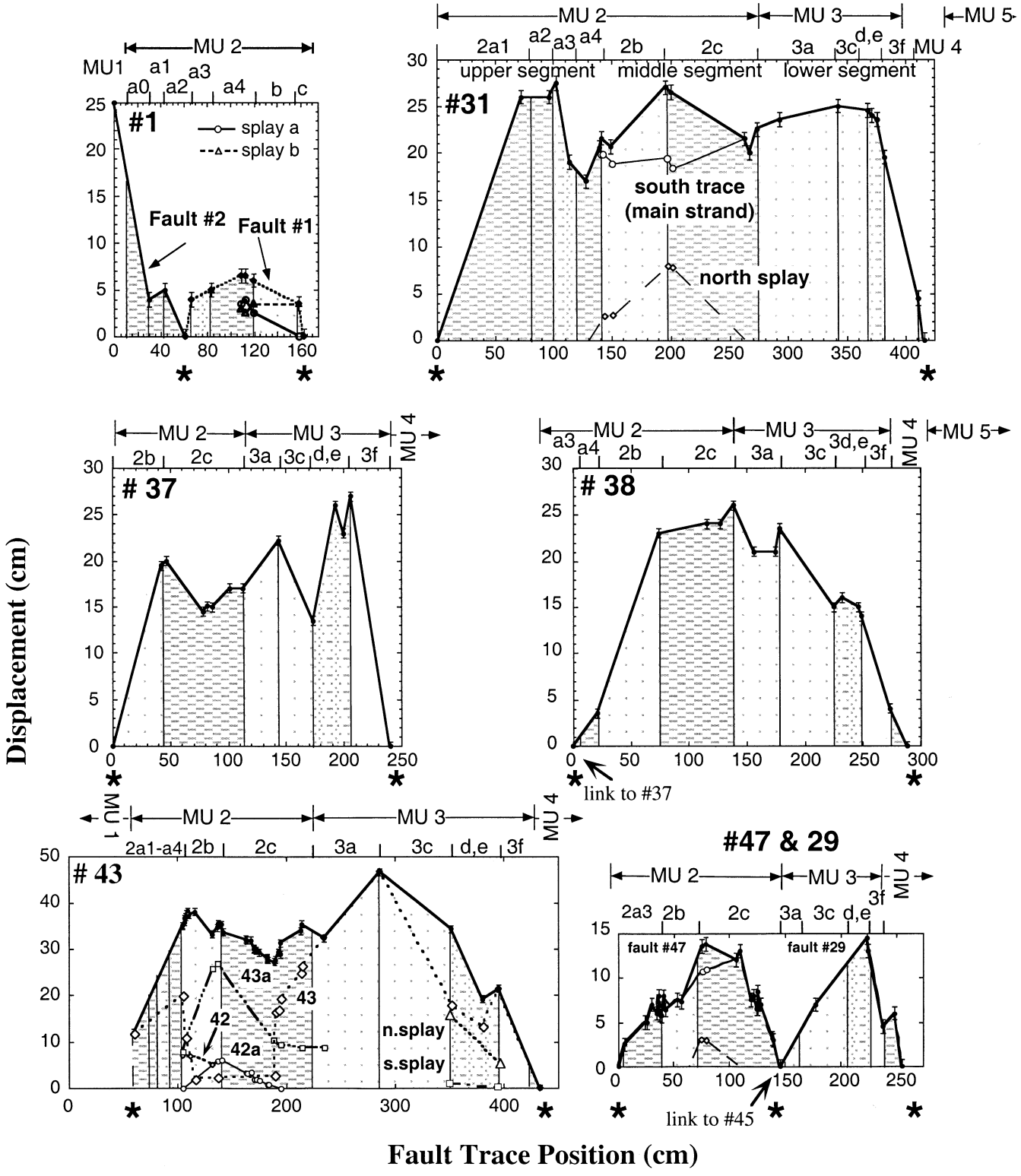

Fig. 7. Displacement profiles of throughgoing faults at Josie's Ranch. Thick lines represent cumulative displacement whereas thin lines represent individual fault traces. Refer to Fig. 4 for key to lithologic patterns and mechanical units, and to Fig. 5 for fault locations. Asterisks represent locations of fault restriction. Error bars are 1.5 cm.

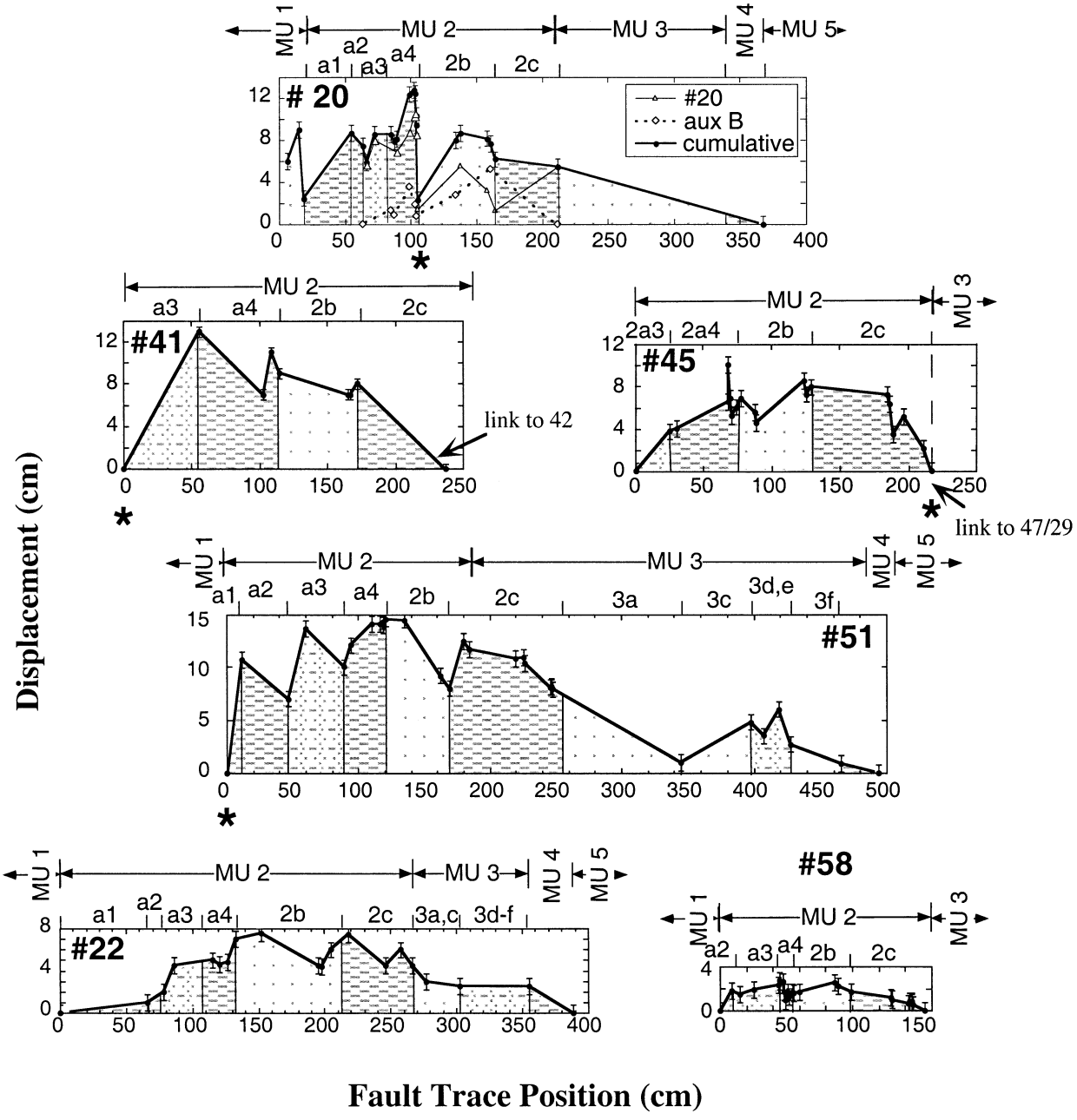

Fig. 7. (*continued*)

cross-section may provide insight into fault growth processes in layered rocks.

4.3.1. Overall scaling relation between displacement and cross-sectional trace length

Maximum displacement is plotted versus cross-sectional trace length on logarithmic scales for all measured faults, both small and large (Fig. 10). The results reveal a positive correlation ($r = 0.75$) with a degree of scatter typical of most D–L datasets. In fact, the data we present from cross-sectional exposures show a comparable amount of scatter, or considerably less scatter, than many individual D–L datasets where length was measured along strike (e.g. Walsh and Watterson, 1988; Peacock and Sanderson, 1991; Cartwright et al., 1995; Dawers and Anders, 1995; Schlische et al., 1996). This further validates our point that displacement–length scaling relations can be observed in a variety of reference planes, including cross-sectional exposures. Furthermore, the cross-sectional perspective allows us to investigate the influence of lithology and the restrictive nature of mechanical layer boundaries on the displacement-length relationship, as demonstrated below.

4.3.2. D_{max}/L ratios as a function of host-rock lithology

Differences in host lithology along fault zones can affect displacement magnitudes, and arise because of differences

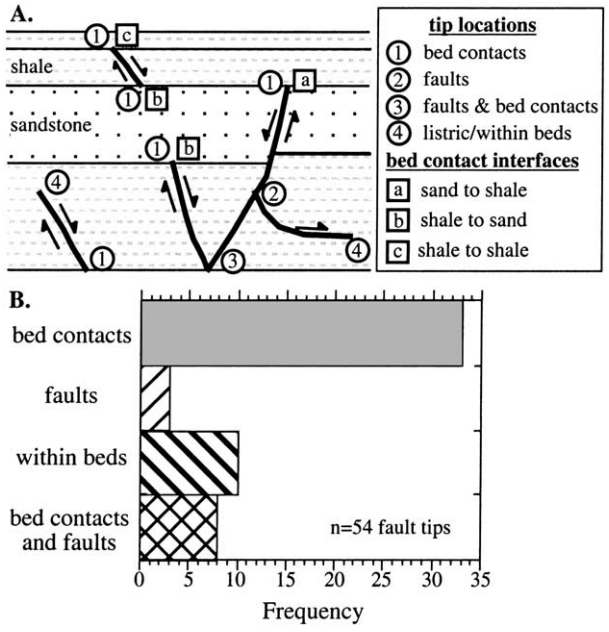

Fig. 8. (A) Schematic illustrating fault tip locations and types of bed contact interfaces. (B) Frequency histogram of fault terminations according to termination location defined in (A). Seven of the 10 fault tips that are found within beds occur within MU 4 and exhibit listric geometries.

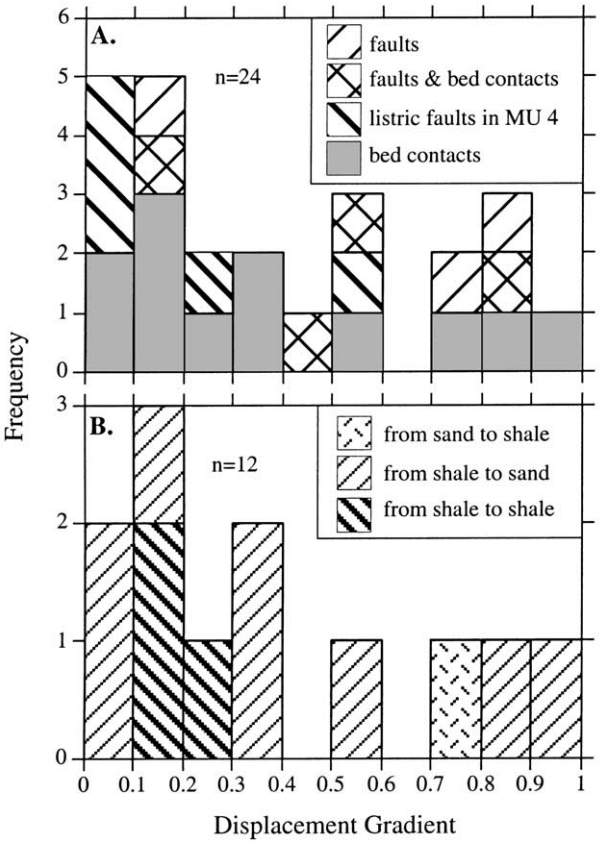

Fig. 9. (A) Histogram of near-tip displacement gradients as classified according to the type of tip restrictor (see Fig. 8A). (B) Histogram of near-tip displacement gradients for different types of bed-contact interfaces. Note how faults with listric tip geometries and faults at shale–shale contacts tend to have lower displacement gradients, but other fault tips have a wide range of gradients.

in rheology that act to modulate the displacement for a given driving stress (e.g. Bürgmann et al., 1994). To test such a relationship, we calculate the percentage of shale host rock that each fault displaces, and compare this with the D_{max}/L ratio calculated for that fault (Fig. 11A). First considering all available fault data, there exists a significant negative correlation between percent shale displaced by a fault and its D_{max}/L ratio ($r = -0.63$ at a significance level of $p < 0.020$). In other words, a greater amount of shale in a faulted section will result in a lower D_{max}/Lratio. We can further isolate the influence of host lithology on the D_{max}/L ratio by excluding three faults that display aberrant levels of fault interaction with mechanical boundaries. For example, fault 47 is restricted from propagating at both tips, and thus exhibits a higher D_{max}/L than expected. Fault 20 is linked with a large joint in overlying MU 1 and thus an accurate D_{max}/L cannot be obtained. Fault 51 has recently linked, and thus the D_{max}/L ratio is much lower than expected. The remaining data yield a very strong negative correlation ($r = -0.91$) between percent shale displaced by a fault and its D_{max}/L ratio, at a significance level of $p < 0.002$.

4.3.3. D_{max}/L ratios as a function of fault tip gradient

We next consider the possibility that mechanical boundaries such as lithologic contacts or pre-existing fault surfaces may serve to restrict fault growth, and thus may influence the displacement–length relationships along faults. This is accomplished by plotting the D_{max}/Lratio as a function of the average tip gradient along a fault (Fig. 11B), the latter calculated by averaging the near-tip displacement gradients at the lower and upper tips along a single fault. First considering all of the data, there is a significant positive correlation between the D_{max}/L ratio and the average fault tip gradient ($r = 0.62$ at a significance level of $p < 0.024$). In order to avoid the influence of other factors, we exclude faults 1 and 31 that displace unusually large sections of shale, as well as fault 51 that soles listrically into MU 4. The remaining data yield a very strong positive correlation ($r = 0.92$) between the average fault tip gradient and its D_{max}/L ratio, at a significance level of $p < 0.001$.

4.3.4. Multiple regression analysis

The results reported above indicate that the D_{max}/L ratio of a fault is a direct function of at least two individual factors, namely the lithology offset by the fault as manifested by the percent shale, and the degree of restriction at the fault tips as manifested by the average tip gradient. We thus performed a multiple regression to explore the possibility that the two factors can be used together to generate a predictive model for the maximum displacement across a fault of given length. The statistical procedure attempts to predict a dependent variable (i.e. the D_{max}/L ratio) as a

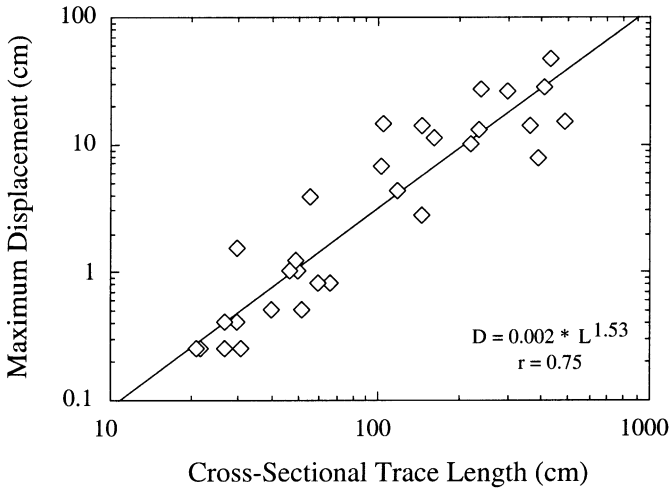

Fig. 10. Logarithmic plot of maximum displacement versus cross-sectional trace length for all measured faults at the Josie's Ranch outcrop.

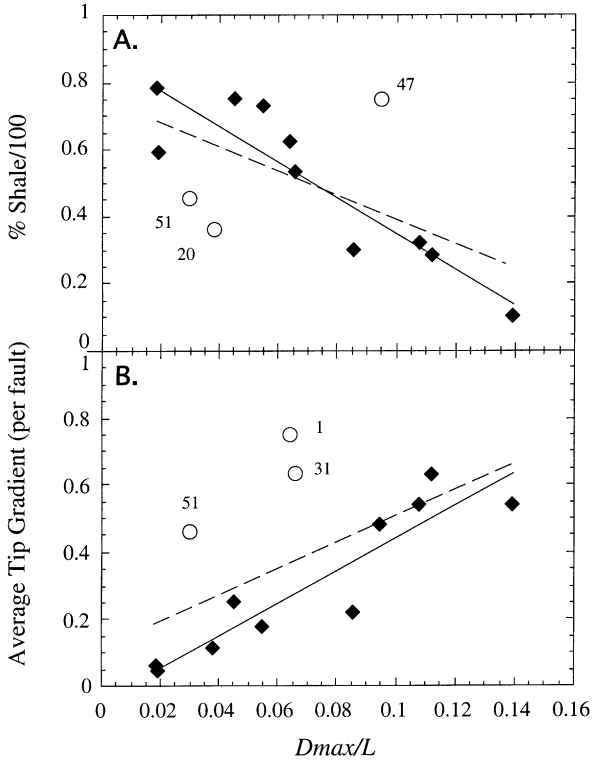

Fig. 11. (A) Plot of percent shale (as a fraction) offset by a fault versus its D_{max}/L ratio. Pearson correlation for entire dataset ($r = -0.634$ at $p < 0.02$); Pearson correlation excluding outliers ($r = -0.910$ at $p < 0.002$). (B) Plot of average fault tip gradient for each fault versus its D_{max}/L ratio. Pearson correlation for entire dataset ($r = -0.621$ at $p < 0.024$); Pearson correlation excluding outliers ($r = 0.916$ at $p < 0.001$). Dashed lines are linear regressions for all data, whereas solid lines represent data excluding outliers (numbered circles). Note that increasing percent shale results in lower D_{max}/L ratios, and increasing fault tip gradients result in higher D_{max}/L ratios. The two correlations are statistically significant, whether or not the outliers are excluded from analysis.

function of two independent variables (i.e. percent shale and average tip gradient). In order to avoid potential bias that may arise from eliminating outlying data points, we first analyze all 13 data. Results of the multiple regression indicate that 60% of the variability of D_{max}/L (as seen in Fig. 10) can be explained by its linear relationship to percent shale and average tip gradient when the two factors are analyzed together. The probability that such a result could have occurred due to chance is less than 0.011. In contrast, percent shale by itself only accounts for 40% of the variability, and average tip gradient by itself only accounts for 38% of the variability. The results provide the following predicted equation for D_{max}/L:

$$D_{max}/L = 0.0823 - 0.0845(S_{pc}) + 0.073(G_{ave}) \quad (1)$$

where D_{max} is maximum displacement along the fault, L is cross-sectional trace length of the fault, S_{pc} is the percent shale displaced by the fault, and G_{ave} is the average fault tip gradient.

We then applied multiple regression to the more limited dataset that excludes the five problematic faults described above. The analysis reveals that 94% of the variability of D_{max}/L can be explained by its linear relationship to percent shale and average tip gradient when analyzed together. The probability that such a result could have occurred due to chance is less than 0.001. When analyzed separately, percent shale and average tip gradient account for 83 and 84% of the variability, respectively. The resulting predicted equation is:

$$D_{max}/L = 0.0829 - 0.0867(S_{pc}) + 0.104(G_{ave}) \quad (2)$$

Note the close similarity in the two equations, suggesting that removal of the outliers did not affect the general relationship among the three variables.

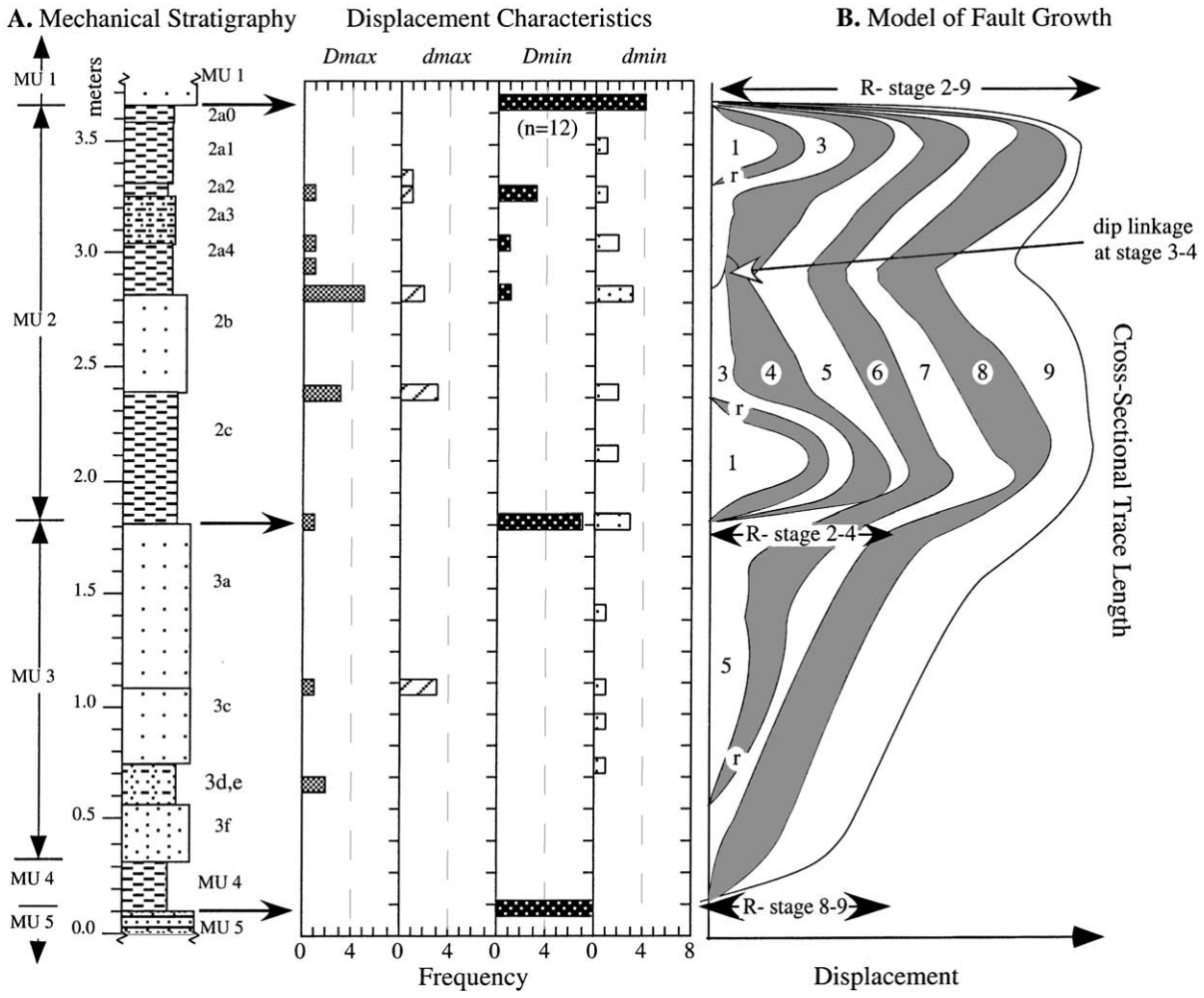

Fig. 12. (A) Histograms of fault attributes (i.e. D_{max}, d_{max}, D_{min}, and d_{min}) plotted as a function of position within the mechanical stratigraphy. Large horizontal arrows indicate major mechanical unit contacts. (B) Barrier growth model showing evolution of displacement profiles for fault growth within the stratigraphic section. (*R*) represents restriction at major mechanical unit barriers while (*r*) represents minor mechanical unit barriers. Numbers next to each profile correspond to each successive stage of fault growth.

5. Discussion

5.1. Influence of mechanical layering on fault development

In order to determine whether fault development is controlled by rock layering, we provide a summary histogram of fault profile attributes (i.e. D_{max}, d_{max}, D_{min}, and d_{min}) plotted as a function of mechanical stratigraphic position (Fig. 12A). In this manner we can evaluate whether certain profile attributes correlate with specific mechanical units, or boundaries between specific mechanical units. These observations, in turn, may provide insight into the evolution of normal fault systems in layered rocks.

5.1.1. Locations of fault initiation

The majority of D_{max} are located within MU 2 (Fig. 12A). Regions of maximum fault displacement often correspond to regions of fault initiation because fault sections near the tips have experienced less slip than the older sections near the zone of initiation (e.g. Elliot, 1976; Ellis and Dunlap, 1988; Walsh and Watterson, 1987). However, variations in elastic properties along a fault as well as interactions with other faults may also influence displacement distributions (Bürgmann et al., 1994; Cowie, 1998; Cowie and Shipton, 1998; Maerten et al., 1999; Schultz, 2000), thus the point of maximum displacement does not necessarily correspond precisely to the point of fault initiation. Nevertheless, the overall abundance of displacement maxima in MU 2 suggests to us that most of the faults initiated somewhere in this shale-rich unit, though we are unable to identify precise points of initiation. Fault initiation in MU 2 is further supported by a large population of small faults confined exclusively to this unit. Considering that large faults evolve from regions of distributed small faults to more localized, throughgoing faults (e.g. Lockner et al., 1992; Gross et al., 1997b; Cowie, 1998; Ackermann et al., 2001), we interpret the region of distributed faulting in MU 2 to represent the general region of fault initiation.

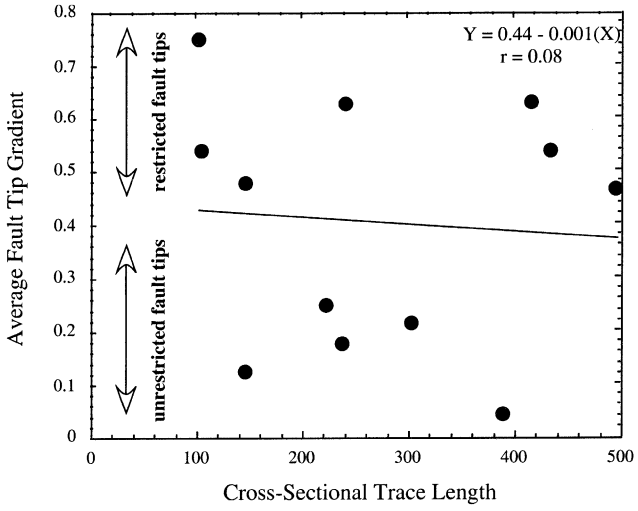

Fig. 13. Plot of average fault tip gradient versus cross-sectional trace length. Note the lack of correlation between the two parameters, and the existence of both high and low tip gradients for a wide range of fault length. This indicates that fault restriction occurs at a variety of scales, most likely in response to the heterogeneous mechanical stratigraphy.

5.1.2. Fault termination and restriction

The largest frequencies of fault tips (D_{mins}) are located at the contacts between major mechanical units (Fig. 12A). This implies that strong contrasts in lithology as well as interfaces at major mechanical unit boundaries serve as prominent barriers to fault growth, often restricting the faults to specific stratigraphic intervals for relatively long periods of time during fault development. The upper tips of faults within MU 2 mostly terminate at the boundary with the overlying, massive sandstone (MU 1). Sharp sandstone–shale transitions at the MU 2–MU 3 and MU 4–MU 5 contacts were also barriers to fault propagation as suggested by the concentration of D_{mins} at these stratigraphic positions (Fig. 12A). Field studies by Rippon (1985) and Peacock (1991) as well as numerical models of Bürgmann et al. (1994) suggest that differences in mechanical properties and contacts between adjacent lithologic units can create effective barriers that inhibit fault propagation.

Several mechanisms have been proposed to explain how barriers to fault propagation are temporary with respect to fault development (Das and Aki, 1977; Cowie and Scholz, 1992c). If external loading conditions remain unchanged, these barriers cannot restrict propagation indefinitely because infinite strains will eventually accumulate near the fault tips (Cowie and Scholz, 1992c; Gupta and Scholz, 2000), thereby leading to propagation across the barrier. If the energy available to create new surface area is proportional to the slip patch dimension (e.g. Cowie and Scholz, 1992a), and assuming that the slip patch dimension is an increasing function of fault length at the scale of the studied faults, then as the fault increases in length, barriers that once were restrictive no longer serve as impediments to fault growth (Cowie and Shipton, 1998). In other words, the active barriers to fault propagation are stronger than other barriers that served to restrict fault growth at earlier stages of fault development (Das and Aki, 1977).

We believe that a similar shift in barrier effectiveness can be observed at the Josie's Ranch outcrop. Numerous small faults have tips residing at minor mechanical unit boundaries (e.g. MU 2a3 and MU 2b), implying that these contacts serve as effective barriers to propagation at early stages of fault development, when cross-sectional trace lengths are small (stages 1–2 in Fig. 12B). For large faults that span more than one mechanical unit, evidence for the restrictive nature of minor mechanical unit boundaries during early stages of fault growth is manifested by the frequency of d_{mins} at these contacts (Fig. 12A). However, tips of large faults are not found at minor mechanical unit contacts, but only at contacts between major mechanical units (Figs. 5, 7 and 12). This suggests to us that as the faults grow in length, minor mechanical unit contacts are no longer effective barriers, and the active barriers to fault propagation are the contacts between major mechanical units (stages 3–9 in Fig. 12B). Evidence for such a switch in scale of barrier effectiveness is indicated by the high frequencies of large fault tips (D_{min}) at major mechanical unit contacts (Fig. 12A and B).

5.1.3. Dip linkage of fault segments

Displacement minima (d_{mins}) are scattered throughout the stratigraphic section, although most are located at minor mechanical unit contacts (Fig. 12A). Eleven of the 18 d_{mins} reside at minor mechanical unit boundaries, mostly within MU 2. The displacement minima may represent points of segment linkage, or alternatively they may be created by differences in elastic moduli between adjacent units (Bürgmann et al., 1994). Additional field observations may help to clarify the significance of displacement minima. Many tips belonging to small faults are located at the same bed boundaries as the d_{min}. This indicates that isolated segments are confined to individual mechanical units prior to linkage. Furthermore, in some profiles the amount of displacement at the d_{min} position is so small relative to other positions along the fault zone (e.g. faults 1, 20, 47/29 and 51) that a non-linkage origin (e.g. contrasting elastic moduli) is inconceivable. Other workers have identified unique geometries characteristic of linked fault segments. One such geometry consists of overlapping fault segments that have linked together (e.g. Dawers and Anders, 1995; Childs et al., 1995; 1996). These linkage geometries are observed in faults 31, 37, 41 and 43. Another unique geometry consists of bends in the fault trace where two fault tips, originally separated by some distance, are linked together by an intermediate segment (Childs et al., 1996). These ' steps' are observed in numerous faults (e.g. faults 1, 15, 22, 37, 38, 43 and 51) and are parallel or subparallel to bedding. Most importantly, they occur precisely at the same contacts as the d_{min}, most prominently at the MU 2–MU 3 contact. In light of the correlation between d_{min} and geometries unique to linkage zones, we conclude that many

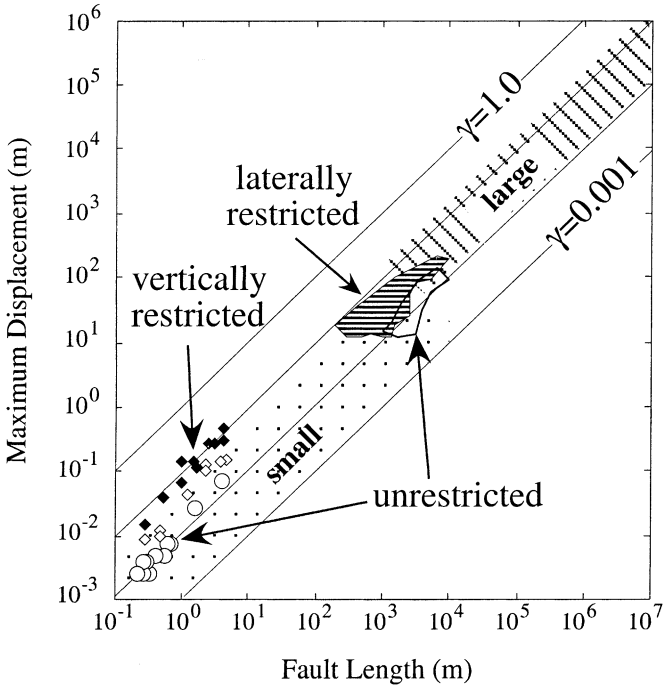

Fig. 14. Logarithmic plot of maximum displacement versus cross-sectional trace length from Josie's Ranch, plotted together with the interpreted global data set of Cowie and Scholz (1992b) and the laterally restricted and unrestricted faults from Nicol et al. (1996). Josie's Ranch data are divided into categories of restricted faults (black diamonds, both fault tips restricted), semi-restricted faults (white diamonds, one tip restricted) and unrestricted faults (white circles, both tips unrestricted). $\gamma = D_{max}/L$. Note the vertically restricted faults at Josie's Ranch have similar D_{max}/L ratios as the 'large' faults of Cowie and Scholz (1992b), implying that mechanical units at the centimeter–meter scale influence fault growth in the same manner as a mechanical unit defined by the seismogenic thickness of the crust.

of the d_{min} correspond to points of fault segment linkage, and that linkage occurred primarily at lithologic boundaries.

Locations of segment linkage are often sites of enhanced permeability (e.g. Cox et al., 1995; Sibson, 1996; Curewitz and Karson, 1997) due to increased fracture density in these regions (e.g. Sibson, 1996; Connolly and Cosgrove, 1999). Vein-hosted mineralization is a direct consequence of increased fluid pressures and the presence of highly-permeable conduits, i.e. a well-connected fracture network. Therefore, regions of down-dip segment linkage may serve as potential targets for the exploration of economic ore deposits.

5.2. Consequences of fault restriction on displacement–length scaling

Barriers to fault growth such as lithologic contacts and intersections with other faults invariably lead to high gradients at fault tips (Ellis and Dunlap, 1988; Peacock, 1991; Peacock and Sanderson, 1991; Cartwright et al., 1995; Dawers and Anders, 1995; Willemse et al., 1996; Morley, 1999), It follows that if displacement continues to accrue across a fault while its tips remain pinned, then the D_{max}/L ratio will increase. This is demonstrated by the correlation between average tip gradients and D_{max}/L for the faults measured in this study (Fig. 11B). This process has also been quantitatively predicted by implementing a reduction in cohesive end-zone size during restricted fault growth (Schultz and Fossen, 2002). Once a fault breaks through a lithologic barrier it becomes unrestricted and the D_{max}/L ratio will decrease. As a fault grows in cross-sectional trace length, it will alternate between a restricted and unrestricted status as it encounters barriers (i.e. mechanical layer boundaries) at a variety of scales (Fig. 12B). One consequence of such a repetitive growth cycle is the lack of correlation between average tip gradient (and hence D/L ratio) and fault length, as well as high and low tip gradients for a wide range of cross-sectional fault lengths (Fig. 13).

When plotted against the interpreted global data set of Cowie and Scholz (1992b), restricted faults measured at this outcrop fall within D–L space presumed to represent only those faults that span the seismogenic regime (Fig. 14), i.e. faults with strike lengths greater than 10 km. In contrast, unrestricted faults fall within the region designated as 'small' faults. This suggests that the seismogenic thickness does not define a unique mechanical layer thickness with respect to D/L. Rather, the effective mechanical layer thickness occurs over a broad range of scales (Becker and Gross, 1996; Wojtal, 1996; Gross et al., 1997b), thus fault growth must be considered together with the mechanical stratigraphy in order to adequately determine D–L scaling relationships, *regardless of the scale of investigation*.

5.3. Predictive models of fault length and displacement

The dependence of D_{max}/L on both rock composition and fault tip gradient, along with corresponding Eqs. (1) and (2) derived from multiple regression analysis, may provide a powerful tool to predict fracture attributes in the subsurface. One long-standing issue confronting geoscientists has been the characterization of fracture and fault systems in subsurface reservoirs and aquifers, with particular interest placed on the prediction of fault dimensions and hydrologic properties at the reservoir-scale (e.g. Childs et al., 1990; Yielding et al., 1996). Many faults that impact fluid flow at the reservoir scale cannot be measured directly, because they are too small to be imaged by seismic surveys on the one hand, yet are incompletely sampled by wellbores on the other hand. Thus, scaling relations based on global datasets and theoretical considerations (e.g. Cowie and Scholz, 1992b; Gauthier and Lake, 1993) have been employed to build fault models at the reservoir scale.

However, fault scaling relations are greatly impacted by a number of factors, including mechanical stratigraphy and localized strain (e.g. Wojtal, 1994; Gross et al., 1997b). We suggest that results from the multiple regression presented in this study can be used to refine models for predicting fault dimensions in the subsurface. Existing subsurface data such as core and well logs can be used to construct a detailed mechanical stratigraphy. Lithologic boundaries that may serve as barriers to fault propagation can be identified at a variety of scales, and serve as the basis for predicting cross-sectional trace lengths and dimensions of fault segments. Knowledge of tectonic history and structural position can provide constraints for estimating degree of restriction in the form of fault tip gradients. Composition of clastic rocks in terms of percent shale versus percent sand can be determined by direct (core analysis) or indirect (geophysical well logs) methods. These estimates, in turn, can be used to model D_{max}/L as a function of rock composition and degree of restriction. Results will facilitate a more accurate assessment of reservoir-scale hydrologic properties such as permeability and connectivity, which can be directly related to attributes of fault populations (e.g. Marrett, 1996).

6. Conclusions

Our analysis of normal fault displacement profiles in cross-section reveals the importance of mechanical layering in controlling fault growth. Propagating faults often temporarily arrest at layer boundaries, thus leading to higher D_{max}/L as faults continue to accumulate displacement while their tips remain pinned. Differences in D_{max}/L exist between restricted and unrestricted faults regardless of fault size, in contrast to the scaling difference proposed for 'large' faults that penetrate the seismogenic thickness of the crust and 'small' faults that do not (Cowie and Scholz, 1992b). Therefore, the effective mechanical layer thickness that controls fault restriction, and as a consequence, D_{max}/L scaling, is important at all scales. The influence of restriction on the D_{max}/L ratio, along with changes in host rock rheology, help explain a portion of the scatter that is typically found in most D–L compilations.

Segment boundaries are often defined based on geometry and/or slip distributions, but without regard for the geologic significance of boundary locations. This study provides direct field evidence for the correlation between specific lithologic contacts within the mechanical stratigraphy and the location of segment boundaries and fault terminations. We suggest that researchers consider the influence of mechanical stratigraphy when estimating the locations and strengths of segment boundaries or slip barriers. In addition, future work should consider quantifying the energy required for faults to propagate across different material boundaries, as this may significantly advance our prediction capabilities of the behavior of slip barriers. Finally, the dependence of D_{max}/L on both rock composition and fault tip gradients, and the resulting equations derived from multiple regression, provide the opportunity to predict fault geometries and attributes in the subsurface.

Acknowledgements

Funding for this project was generously provided by grants from the Petroleum Research Fund (ACS-PRF no. 28338-GB2) and the United States–Israel Binational Science Foundation (grant no. 94-00396). Mike Wacker provided valuable field assistance, and we benefited from discussions with Grenville Draper, Terry Engelder, Yehuda Eyal, and Richard Schultz. We thank Paulette Johnson from the FIU Statistics Department for providing the multiple regression analysis. Paul Gillespie, Peter Hennings, and James Evans are thanked for their insightful reviews.

References

Becker, A., Gross, M.R., 1996. Mechanism for joint saturation in mechanically layered rocks: an example from southern Israel. Tectonophysics 257, 223–237.

Bürgmann, R., Pollard, D.D., Martel, S.J., 1994. Slip distributions on faults: effects of stress gradients inelastic deformation, heterogeneous host-rock stiffness, and fault interaction. Journal of Structural Geology 16, 1675–1690.

Cartwright, J.A., Mansfield, C.M., 1998. Lateral displacement variations and lateral tip geomety of normal faults in the Canyonlands National Park, Utah. Journal of Structural Geology 20, 3–19.

Cartwright, J.A., Trudgill, B.D., Mansfield, C.M., 1995. Fault growth by segment linkage: an explanation for scatter in maximum displacement and trace length data from the Canyonlands Grabens of S.E. Utah. Journal of Structural Geology 17, 1319–1326.

Caskey, S.J., Wesnousky, S.G., Zhang, P., Slemmons, D.B., 1996. Surface faulting of the 1954 Fairview Peak (Ms 7.2) and Dixie Valley (Ms 6.8) earthquakes, central Nevada. Bulletin of the Seismological Society of America 86, 761–787.

Childs, C., Walsh, J.J., Watterson, J., 1990. A method for estimation of the density of fault displacements below the limit of seismic resolution in

reservoir formations. In: Buller, A.T., Berg, E., Hjelmeland, O., Kleppe, J., Torsaeter, O., Aasen, J.O. (Eds.). North Sea Oil and Gas Reservoirs II. Graham and Trotman, London, pp. 309–318.

Childs, C., Watterson, J., Walsh, J.J., 1995. Fault overlap zones within developing normal fault systems. Journal of the Geological Society of London 152, 535–549.

Childs, C., Nicol, A., Walsh, J.J., Watterson, J., 1996. Growth of vertically segmented normal faults. Journal of Structural Geology 18, 1389–1397.

Clark, R.M., Cox, S.J.D., 1996. A modern regression approach to determining fault displacement–length scaling relationships. Journal of Structural Geology 18, 147–152.

Connolly, P., Cosgrove, J., 1999. Prediction of fracture induced permeability and fluid flow in the crust using experimental stress data. American Association of Petroleum Geologists Bulletin 83, 757–777.

Corbett, K., Friedman, M., Spang, J., 1987. Fracture development and mechanical stratigraphy of Austin Chalk, Texas. American Association of Petroleum Geologists Bulletin 71, 17–28.

Cowie, P.A., 1998. A healing–reloading feedback control on the growth rate of seismogenic faults. Journal of Structural Geology 20, 1075–1087.

Cowie, P.A., Scholz, C.H., 1992a. Physical explanation for the displacement–length relationship of faults using a post-yield fracture mechanics model. Journal of Structural Geology 14, 1133–1148.

Cowie, P.A., Scholz, C.H., 1992b. Displacement–length scaling relationships for faults: data synthesis and discussion. Journal of Structural Geology 14, 1149–1156.

Cowie, P.A., Scholz, C.H., 1992c. Growth of faults by accumulation of seismic slip. Journal of Geophysical Research 97, 11085–11095.

Cowie, P.A., Shipton, Z., 1998. Fault tip displacement gradients and process zone dimensions. Journal of Structural Geology 20, 983–997.

Cox, S.F., Sun, S.S., Etheridge, M.A., Wall, V.J., Potter, T.F., 1995. Structural and geochemical controls on the development of turbidite-hosted gold quartz vein deposits, Wattle Gully Mine, central Victoria, Australia. Economic Geology and the Bulletin of the Society of Economic Geologists 90, 1722–1746.

Curewitz, D., Karson, J.A., 1997. Structural settings of hydrothermal outflow; fracture permeability maintained by fault propagation and interaction. Journal of Volcanology and Geothermal Research 79, 149–168.

Das, S., Aki, K., 1977. Fault plane with barriers; a versatile earthquake model. Journal of Geophysical Research 82, 5658–5670.

Dawers, N.H., Anders, M.H., 1995. Displacement–length scaling and fault linkage. Journal of Structural Geology 17, 607–614.

Dawers, N.H., Anders, M.H., Scholz, C.H., 1993. Growth of normal faults: displacement–length scaling. Geology 21, 1107–1110.

Doutsos, T., Poulimenos, G., 1992. Geometry and kinematics of active faults and their seismotectonic significance in the western Corinth–Patras rift (Greece). Journal of Structural Geology 14, 689–699.

Elliot, D., 1976. The energy balance and deformation mechanism of thrust sheets. Philosophical Transactions of the Royal Society of London A283, 289–312.

Ellis, M.A., Dunlap, W.J., 1988. Displacement variation along thrust faults: implications for the development of large faults. Journal of Structural Geology 10, 183–192.

Engelder, T., Gross, M.R., Pinkerton, P., 1997. Joint development in clastic rocks of the Elk Basin anticline, Montana–Wyoming: an analysis of fracture spacing versus bed thickness in a basement-involved Laramide structure. In: Hoak, T.E., Klawitter, A.L., Blomquist, P.K. (Eds.). Fractured Reservoirs; Characterization and Modeling. Rocky Mountain Association of Geologists, Denver, CO, pp. 1–18.

Fischer, M.P., Jackson, P.B., 1999. Stratigraphic controls on deformation patterns in fault-related folds: a detachment fold example from the Sierra Madre Orientale, northeast Mexico. Journal of Structural Geology 21, 613–633.

Gauthier, B.D.M., Lake, S.D., 1993. Probabilistic modeling of faults below the limit of seismic resolution in Pelican Field, North Sea, offshore United Kingdom. American Association of Petroleum Geologists Bulletin 77, 761–777.

Gregson, J.D., Erslev, E.A., 1997. Heterogeneous Laramide deformation in the Uinta Mountains, Colorado and Utah. In: Hoak, T.E., Klawitter, A.L., Blomquist, P.K. (Eds.). Fractured Reservoirs; Characterization and Modeling. Rocky Mountain Association of Geologists, Denver, CO, pp. 137–154.

Gross, M.R., 1995. Fracture partitioning: failure mode as a function of lithology in the Monterey Formation of coastal California. Geological Society of America Bulletin 107, 779–792.

Gross, M.R., Becker, A., Gutierrez-Alonso, G., 1997a. Transfer of displacement from multiple slip zones to a single detachment due to rigid block rotation: example from the Dead Sea Rift, Israel. Geological Society of America Bulletin 109, 1021–1035.

Gross, M.R., Gutiérrez-Alonso, G., Bai, T., Wacker, M.A., Collinsworth, K.B., Behl, R.J., 1997b. Influence of mechanical stratigraphy and kinematics on fault scaling relations. Journal of Structural Geology 19, 171–183.

Gross, M.R., Bahat, D., Becker, A., 1997c. Relations between jointing and faulting based on fracture-spacing ratios and fault-slip profiles: a new method to estimate strain in layered rocks. Geology 25, 887–890.

Gupta, A., Scholz, C.H., 2000. A model of normal fault interaction based on observations and theory. Journal of Structural Geology 22, 865–879.

Lockner, D.A., Byerlee, J.D., Kuksenko, V., Ponomarev, A., Sidorin, A., 1992. Observations of quasistatic fault growth from acoustic emissions. In: Evans, B., Wong, T.-F. (Eds.). Fault Mechanics and Transport Properties of Rocks. Academic Press, London, pp. 3–31.

Maerten, L., Willemse, E.J.M., Pollard, D.D., Rawnsley, K.D., 1999. Slip distributions on intersecting normal faults. Journal of Structural Geology 21, 259–271.

Mansfield, C.S., Cartwright, J.A., 1996. High resolution fault displacement mapping from three-dimensional seismic data: evidence for dip linkage during fault growth. Journal of Structural Geology 18, 249–263.

Marrett, R., 1996. Aggregate properties of fracture populations. Journal of Structural Geology 18, 169–178.

Marrett, R., Allmendinger, R.W., 1991. Estimates of strain due to brittle faulting. Journal of Structural Geology 13, 735–738.

McConnell D.A., Wilson, T.G., 1993. Linkage between deformation of basement rocks and sedimentary rocks in basement-involved foreland folds. In: Schmidt, C.J., Chase, R.B., Erslev, E.A. (Eds.), Laramide Basement Deformation in the Rocky Mountain Foreland of the Western United States. Geological Society of America, Special Paper 280, pp. 319–333.

Moore, J.M., Schultz, R.A., 1999. Process of faulting in jointed rocks of Canyonlands National Park, Utah. Geological Society of America Bulletin 111, 808–822.

Morley, C.K., 1999. Patterns of displacement along large normal faults: implications for basin evolution and fault propagation, based on examples from East Africa. American Association of Petroleum Geologists Bulletin 83, 613–634.

Muraoka, H., Kamata, H., 1983. Displacement distribution along minor fault traces. Journal of Structural Geology 5, 483–495.

Nicol, A., Watterson, J., Walsh, J.J., Childs, C., 1996. The shapes, major axis orientations and displacement patterns of fault surfaces. Journal of Structural Geology 18, 235–248.

Opheim, J.A., Gudmundsson, A., 1989. Formation and geometry of fractures, and related volcanism, of the Krafla fissure swarm, northeast Iceland. Geological Society of America Bulletin 101, 1608–1622.

Peacock, D.C.P., 1991. Displacement and segment linkage in strike-slip fault zones. Journal of Structural Geology 13, 1025–1035.

Peacock, D.C.P., Sanderson, D.J., 1991. Displacements, segment linkage and relay ramps in normal fault zones. Journal of Structural Geology 13, 721–733.

Peacock, D.C.P., Zhang, X., 1994. Field examples and numerical modeling of oversteps and bends along normal faults in cross-section. Tectonophysics 234, 147–167.

Peacock, D.C.P., Sanderson, D.J., 1996. Effects of propagation rate on

displacement variations along faults. Journal of Structural Geology 18, 311–320.

Peacock, D.C.P., Knipe, R.J., Sanderson, D.J., 2000. Glossary of normal faults. Journal of Structural Geology 22, 291–305.

Poulimenos, G., 2000. Scaling properties of normal fault populations in the western Corinth Graben, Greece: implications for fault growth in large strain settings. Journal of Structural Geology 22, 307–322.

Rippon, J.H., 1985. Countoured patterns of throw and shade of normal faults in the Coal Measures (Westphalian) of north-east Derbyshire. Proceedings of the Yorkshire Geological Society 45, 147–161.

Rowley, P.D., Hansen, W.R., 1979. Geologic map of the Split Monument Quadrangle, Uinta County, Utah. U.S. Geological Survey Map GQ-1515, scale 1:24,000.

Rowley, P.D., Hansen, W.R., Tweto, O., Carrara, P.E., 1985. Geologic map of the Vernal $1^\circ \times 2^\circ$ quadrangle, Colorado, Utah, and Wyoming. U.S. Geological Survey Map I-1526, scale 1:250,000.

Schlische, R.W., Young, S.S., Ackermann, R.V., Gupta, A., 1996. Geometry and scaling relations of a population of very small rift-related normal faults. Geology 24, 683–686.

Schultz, R.A., 2000. Understanding the process of faulting: selected challenges and opportunities at the edge of the 21st century. Journal of Structural Geology 21, 985–993.

Schultz, R.A., Fossen, H., 2002. Displacement–length scaling in three-dimensions: the importance of aspect ratio and application to deformation bands. Journal of Structural Geology 24, 1389–1411.

Sibson, R.H., 1996. Structural permeability of fluid-driven fault–fracture meshes. Journal of Structural Geology 18, 1031–1042.

Silliphant, L.J., Engelder, T., Gross, M.R., 2002. The state of stress in the limb of Split Mountain anticline, Utah: constraints placed by transected joints. Journal of Structural Geology 24, 155–172.

Untermann, G.E., Untermann, B.R., 1965. Geologic map of the Dinosaur National Monument, Colorado–Utah. Utah Geological Society, scale 1:62,500.

Walsh, J.J., Watterson, J., 1987. Distributions of cumulative displacement and seismic slip on a single normal fault surface. Journal of Structural Geology 9, 1039–1046.

Walsh, J.J., Watterson, J., 1988. Analysis of the relationship between displacements and dimensions of faults. Journal of Structural Geology 10, 239–247.

Watterson, J., 1986. Fault dimensions, displacements, and growth. Pure and Applied Geophysics 24, 365–373.

Wilkins, S.J., 1999. The influence of mechanical layering on the evolution of brittle structures: fracture partitioning and fault growth in the Glen Canyon Sandstone, Split Mountain, Utah, M.S. thesis, Florida International University, Miami, FL.

Wilkins, S.J., Gross, M.R., Wacker, M., Eyal, Y., Engelder, T., 2001. Faulted joints: kinematics, displacement–length scaling relations, and criteria for their identification. Journal of Structural Geology 23, 315–327.

Willemse, E.J.M., Pollard, D.D., Aydin, A., 1996. Three-dimensional analyses of slip distributions on normal fault arrays with consequences for fault scaling. Journal of Structural Geology 18, 295–309.

Wojtal, S.F., 1994. Fault scaling laws and the temporal evolution of fault systems. Journal of Structural Geology 16, 603–612.

Wojtal, S.F., 1996. Changes in fault displacement populations correlated to linkage between faults. Journal of Structural Geology 18, 265–279.

Yielding, G., Jackson, J.A., King, G.C.P., Sinvhal, H., Vita-Finzi, C., Wood, R.M., 1981. Relations between surface deformation, fault geometry, seismicity, and rupture characteristics during the El Asnam (Algeria) earthquake of 10 October 1980. Earth and Planetary Science Letters 56, 287–304.

Yielding, G., Needham, T., Jones, H., 1996. Sampling of fault populations using sub-surface data: a review. Journal of Structural Geology 18, 135–146.